J. Fluid Mech. (1966), *vol.* 24, *part* 4, *pp.* 625-640
Printed in Great Britain

The starting process in a hypersonic nozzle

By C. EDWARD SMITH

Department of Engineering Science, University of Oxford, England
and Lockheed Missiles and Space Company, Palo Alto, California

(Received 30 July 1965)

This paper describes an experimental study of the starting process in a reflected-shock tunnel, and compares the results with numerical calculations reported previously (Smith 1962). It is shown that an unsteady expansion wave dominates the transient flow, and the shock-wave system plays a minor role. The effects of initial pressure in the nozzle were investigated, and the behaviour of the secondary shock wave was noted. It was found that initial pressures larger even than the steady-flow static pressure can be tolerated without prolonging the starting process, despite the presence of a strong secondary shock wave. Other analyses, based on the 'steady-state' model of the starting process, are discussed and shown to give an unrealistic description of the flow field.

1. Introduction

The unsteady flow that occurs during the starting process of a hypersonic nozzle is important in short-duration facilities. The starting transient decreases the useful testing time of a facility, and an excessively long starting process severely limits its usefulness. A number of investigators have analysed the starting process for a shock-tunnel nozzle, but most have attacked the problem by means of the so-called 'steady-state' model. In this approach, the unsteady flow field behind the starting shock wave is patched to the nozzle steady-flow conditions by means of an upstream-facing disturbance. The path history of the starting shock wave through the nozzle must be known from experimental measurements, or from some approximate theory. At each location in the nozzle the pressure behind this shock wave is matched to the steady-flow static pressure at that location by inserting an upstream-facing shock wave or expansion wave, as required. In this manner the secondary wave and its path history are computed. Parks (1952), Henshall & Gadd (1956), Henshall (1960), and Ackroyd (1964) have applied this method to the starting process in both reflected and non-reflected shock tunnels. It should be noted that the 'steady-state' model *assumes* that steady flow exists in the nozzle as soon as the upstream-facing wave has gone by.

The only analysis that we have found in which a detailed calculation of the entire flow field was made is by Glick, Hertzberg & Smith (1955) and Hertzberg (1956), as applied only to the non-reflected shock tunnel. They used the method of characteristics and demonstrated agreement with experiments. One of their conclusions, which is also substantiated by the 'steady-state' model, was that the initial pressure in the divergent portion of the nozzle must be extremely low to

obtain rapid starting. This is necessary to weaken the secondary wave sufficiently, in order that it be swept through the nozzle as fast as possible, i.e. as a sound wave. This principle is restated by Wittliff, Wilson & Hertzberg (1959) and by Glass & Hall (1959). Values of initial pressure ranging from 0·1 to 5 μ Hg have been used by these workers to minimize the starting time.

It is evident that very low initial pressures do result in rapid starting, but the question remains of how high the initial pressure can be before a loss of testing time occurs. The 'steady-state' model cannot give a satisfactory answer to this question, and it also fails to explain certain experimental observations. Holder & Schultz (1962) reported measurements of the development of the boundary layer on a flat plate for different operating conditions of their shock tunnel. While the 'steady-state' model of the nozzle starting process predicted a thinning of the boundary layer with time only if there was an upstream-facing expansion wave (and a thickening with a shock wave), the boundary layer was found always to become thinner. Many workers, including the present author, have noted that nozzles start just as quickly with initial pressures considerably higher than the foregoing recommendations. Sufficient doubt existed as to the role of the secondary shock wave, the influence of initial nozzle pressure, and the values of flow variables during the starting process for the present work to be initiated.

The analytical work was reported earlier (Smith 1962, 1964), and is briefly summarized below. The present experimental results are compared with the calculations, and the validity of both the theoretical model and the computed flow field is demonstrated. The finding of Smith (1962, 1964), that the duration of the starting process is dominated by the passage of an unsteady expansion wave rather than the two-shock system, is verified experimentally. Finally, the influence of nozzle initial pressure on the behaviour of the secondary shock wave is shown, and the pressure for optimum starting is noted. It is also shown that initial pressures larger even than the steady-flow static pressure do not necessarily cause a loss of steady-flow test time, despite the presence of a strong secondary shock wave.

A list of symbols used throughout this paper is given below:

a	sound speed	β	tangent of nozzle half-angle
A	nozzle area	γ	specific heat ratio, 7/5
c	constant	δ	boundary-layer thickness
M	Mach number	ρ	density
p	pressure		
r_t	throat radius	Subscripts	
R_x	Reynolds number based on x	$( )_e$	value at edge of boundary layer
t	time	$( )_t$	value at nozzle throat
u	flow velocity	$( )_w$	value at flat-plate surface
x	distance	$( )_5$	value in stagnation chamber

2. Theory

2.1. *Flow model*

The present work concerns itself with the starting process in reflected-shock and Hotshot-type tunnels, in which the flow at the nozzle throat is sonic. A diaphragm

was assumed to be at the nozzle throat, which permitted the use of arbitrary initial pressures in the nozzle. Non-reflected shock tunnels, in which there is supersonic flow at the nozzle entrance, were not considered, although the present methods could easily be extended to include them.

A model of the starting process in a nozzle can be constructed by analogy to the flow in a conventional shock tube with two special features; namely, a heated driver, and an area change at the diaphragm. Figure 1 shows the x–t diagram for a pressure ratio sufficiently high to sustain supersonic flow in the nozzle. Flow in region 5 (either behind the reflected shock wave or in the hotshot arc-chamber)

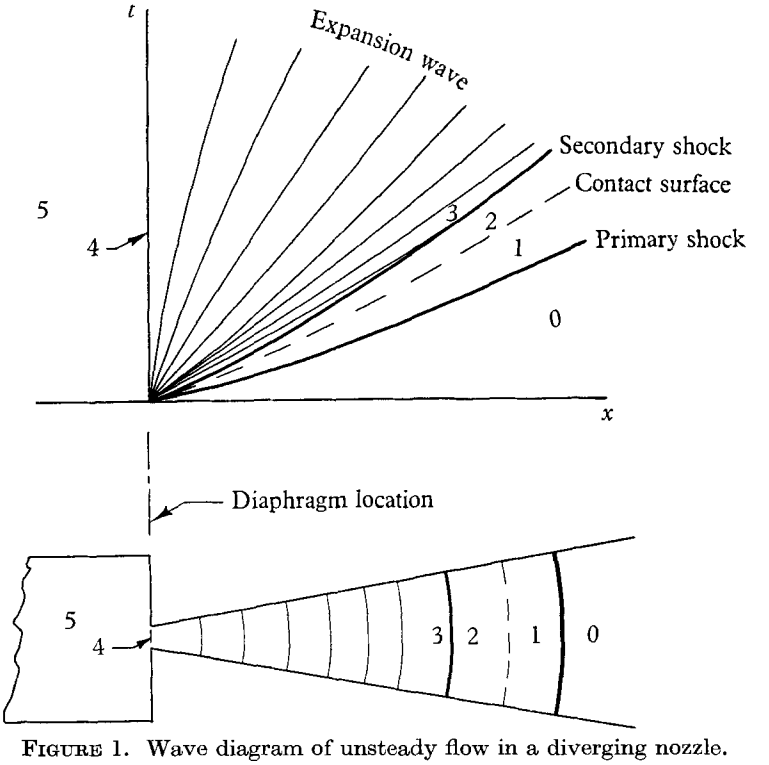

FIGURE 1. Wave diagram of unsteady flow in a diverging nozzle.

undergoes steady expansion from near quiescence to sonic conditions at the throat, 4, then passes through an unsteady expansion wave to some high Mach number in region 3. The presence of this expansion wave is the major difference between this flow model and the 'steady-state' model. The extent of the expansion wave and the initial speed of the transmitted shock wave can be computed from the equations of Alpher & White (1958).

As the shock wave and contact surface move down the diverging nozzle, the interaction with the area change causes the shock wave to decelerate, as reported by Chisnell (1957) and Chester (1960). Behind the decelerating shock wave the value of $(u–a)$ decreases, which causes the minus characteristics in region 1 to rotate progressively (counter-clockwise in figure 1), and to become convergent. This effect also appears in region 2, and a secondary shock wave, initially located at the tail of the unsteady expansion wave (Smith 1962), must appear within the

flow field. The secondary shock wave is at first very weak, but its Mach number increases rapidly with distance. Although this shock wave moves upstream relative to the fluid, its net motion is down the nozzle because of the high flow velocity.

2.2. *Numerical calculations*

For simplicity a perfect gas with $\gamma = 7/5$ was assumed, and the effects of viscosity and heat transfer to the nozzle were neglected. The usual one-dimensional assumption, that the flow variables depend on only one space co-ordinate (axial distance along the nozzle), was made. A boundary condition of constant flow properties at the throat was imposed. A digital-computer program, fully described elsewhere (Smith 1962), was written, which solved the unsteady flow field, numerically utilizing the method of characteristics. The flow in a conical nozzle was computed for three cases with various pressure and temperature ratios. The solution showed that at a given location the duration of the flow between the two shock waves is very short compared with the time required for the unsteady expansion to pass by. The solutions also indicated that the flow velocity during the starting transient is higher, and the acoustic velocity (or static temperature) is lower than the steady-flow values. In all cases strong secondary shock waves were found, although the 'steady-state' model predicts an expansion wave for the high pressure ratios (about 10^6) used in the calculations.

As a comparison with the more detailed calculation, the work of Chisnell (1957) offers an approximate method for computing the path history of a shock wave in a diverging nozzle. The method uniquely relates the Mach number of the shock wave to the nozzle area ratio by neglecting disturbances that overtake the shock wave from behind. If the Mach number is known at some reference location (say, the throat), the value at other locations is given by

$$(M^2-1) = (M_t^2-1)\,(A_t/A)^k \tag{1}$$

for strong shock waves, where k is approximately 0·40 for $\gamma = 1{\cdot}4$.

2.3. *Duration of unsteady flow*

With the aid of these unsteady-flow solutions we can determine the time at which steady flow is obtained in the nozzle. Since the value of $(u-a)$ is greater during the starting transient than in steady flow, all minus characteristics contained in the unsteady expansion wave (between 3 and 4 in figure 1) must arrive at a given nozzle location sooner than the minus characteristic for steady flow. Consequently, the time for the steady-flow characteristic to travel from the throat to some location, given by

$$t = \int_0^x \frac{dx}{a(M-1)}, \tag{2}$$

is the earliest time at which steady flow can exist in the nozzle. The steady-flow equations,

$$A/A_t = \frac{1}{M}\left[\frac{2}{\gamma+1} + \frac{\gamma-1}{\gamma+1}\,M^2\right]^{(\gamma+1)/2(\gamma-1)}, \tag{3}$$

and

$$a_5/a = (1+\tfrac{1}{2}(\gamma-1)\,M^2)^{\frac{1}{2}}, \tag{4}$$

and an equation for $A(x)$ can be combined to evaluate equation (2). The shape of any smooth nozzle near the throat is approximated by

$$A/A_t = 1 + cx^2 + O(x^3), \tag{5}$$

since $(dA/dx)_{x=0}$ must be zero for a throat to exist. This nozzle shape, when used in evaluating equation (2), produces a singularity at $x = 0$, and no finite value of the integral can be found. This result implies that based on a one-dimensional, unsteady model, the nozzle never achieves steady flow, but instead approaches steady flow in an asymptotic manner. A similar behaviour occurs in boundary-layer flow where the free-stream velocity is never attained, but is approached asymptotically.

Because of the singular behaviour of equation (2), it is necessary to make some arbitrary assumption to obtain a value of time after which the flow is 'for practical purposes' steady. Ackroyd (1964), for example, averaged the value of $(u–a)$ over a small distance to begin his integration of equation (2). This technique is objected to because the value of the integral depends on the size of the initial step. The integral increases without bounds as the step size approaches zero. Glick *et al.* (1955) eliminated the singular behaviour by using a wedge-shaped nozzle, which has $dA/dx \neq 0$ at the throat. More precisely, the slope of the nozzle wall changes abruptly at the throat from zero to a value equal to the wedge angle. For wedge- and cone-shaped nozzles equation (2) is not singular, and can be integrated for a particular choice of area and γ. For a conical nozzle whose area is given by

$$A/A_t = (1 + \beta x/r_t)^2 \tag{6}$$

and a γ of 7/5, the result is

$$t = \frac{0{\cdot}76 r_t}{\beta a_5}\left[M^{\frac{1}{2}}\left(1 - \frac{1}{M}\right) + \tfrac{1}{15}(M^{\frac{3}{2}} - 1) + \tfrac{1}{25}(M^{\frac{5}{2}} - 1)\right]. \tag{7}$$

This expression, too, is based on an arbitrary assumption, concerning the shaping of the nozzle at the throat. It therefore does not represent the time at which steady flow is achieved, but yields an estimate of a 'time of close approach' to steady flow. It can be seen that large nozzle angles, small throat sizes, and high stagnation temperatures lead to short starting transients for a given flow Mach number. Naturally, the foregoing analysis is valid only if the secondary shock wave has passed by the nozzle station of interest before the time given by equation (7).

2.4. *Behaviour of the secondary shock wave*

The differences in behaviour of the secondary shock wave in the 'steady-state' model and the present work can now be discussed. In the 'steady-state' model this shock wave is allowed to originate along the $(u–a)$ characteristic appropriate to steady flow in the nozzle. If it did not grow in strength, but remained an acoustic wave, its time of arrival at any location in a conical nozzle would be given by equation (7). Any increase of strength would cause the shock wave to arrive later, and a corresponding loss of testing time would occur. Under no conditions could it arrive at a nozzle location sooner than the time predicted by equation (7).

With the present flow model the secondary shock wave must be placed at the tail of an unsteady expansion wave, as shown in figure 1. Although the strength of this shock wave increases as it moves through the nozzle, the shock wave must travel across the unsteady expansion wave before it can cause a loss of testing time. Consequently, a strong secondary shock wave can be present and cause no loss providing it does not completely cross the expansion wave while being swept through the nozzle.

2.5. *Unsteady approach to steady flow*

The secondary shock wave marks the limit of upstream influence that the initial conditions in the nozzle have on the subsequent flow. This shock wave may propagate various distances into the expansion wave depending on initial conditions, but the remaining part of the expansion wave is unaffected by the initial conditions. The unaffected portion of the unsteady flow depends only on upstream conditions, and can be computed (Smith 1962, 1964) without accounting for the primary and secondary shock wave. In fact, similarity considerations reveal that the unsteady approach to steady flow in a given nozzle is the same for all values of initial pressure and temperature ratio if the solution is expressed in terms of a/a_5, u/a_5 and p/p_5 as functions of x/r_t and $a_5 t/r_t$. For a given nozzle shape a single numerical solution describes the approach to steady flow for all operating conditions. For the special case of a conical nozzle, use of the independent variables $\beta x/r_t$ and $\beta a_5 t/r_t$ removes the effect of nozzle cone angle, and solutions computed with one value of cone angle can easily be modified to apply to a nozzle having another angle.

3. Experiments

3.1. *Apparatus and procedure*

The shock tunnel in which these data were obtained comprised a $1\frac{7}{8}$ in. diameter, stainless-steel shock tube terminated by a brass nozzle. An unscribed aluminium diaphragm separated the 3 ft. driver section from the 11 ft. driven section. The nozzle, shown in figure 2, had a flat front surface to reflect the incident shock wave, a smooth convergence to a 0·2 in. diameter throat, and a conical diverging section with a half-angle of 10°. The entrance portion was detachable, to permit a Melinex diaphragm with a thickness of 0·00025 in. to be placed at the throat for all tests. The distance from the throat to the nozzle exit was 5 in., and the area ratio at the exit was almost 100. The nozzle delivered a free jet into a large test section. The test section, which had windows to permit flow visualization by schlieren photography, was followed by a dump tank.

The arrival of the incident shock wave was detected at 28, 16 and 4 in. before the end of the driven tube by means of thin-film heat-transfer gauges, and the time of passage from one gauge to another was displayed on two microsec-counter chronometers. The average speed of the shock wave between gauges was computed, and used to determine the time at which the shock wave reached the end of the driven tube, as well as its Mach number upon arrival. The time of shock reflexion was taken as zero datum, and all timing data were suitably adjusted. A Kistler pressure gauge, mounted $\frac{1}{2}$ in. from the end of the driven tube, measured

the pressure behind the reflected shock wave, and gave additional timing data for the shock waves. Its signal was passed through a charge amplifier and displayed with an oscilloscope.

The time history of the primary (starting) shock wave through the nozzle was measured with a probe fabricated from a $\frac{1}{4}$ in. diameter Pyrex tube. The tube was heated and drawn into a conical shape, and three thin-film heat-transfer gauges were placed around the outside at 1·5 in. intervals. The gauges were about $\frac{3}{8}$ in. long, and had a width of less than $\frac{1}{16}$ in. in the flow direction. Each gauge had a resistance of about 100 ohms, and was powered by means of wires run inside

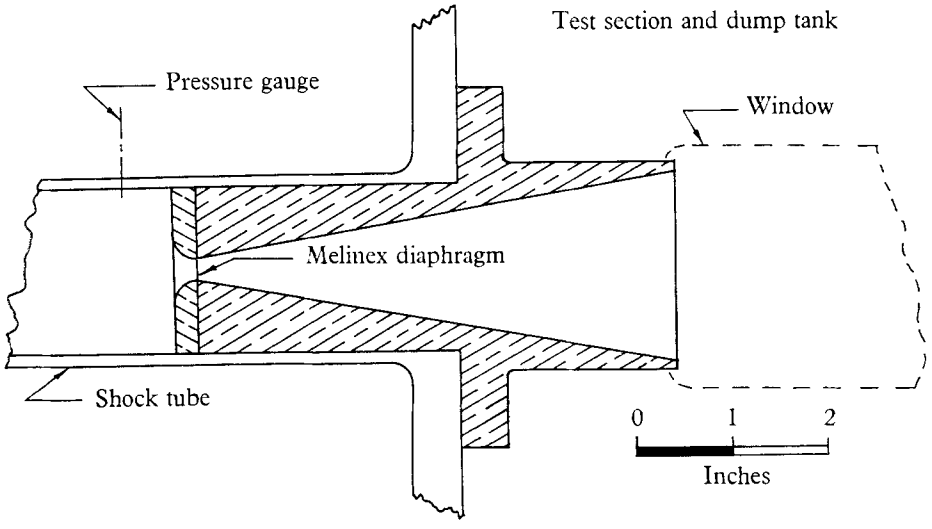

FIGURE 2. Scale drawing of shock-tunnel nozzle.

the tube and brought through holes near the gauges. A current of approximately 20 mA was passed through each gauge, and the gauge voltages were displayed directly on oscilloscopes. The shock arrival time could be determined within 1–2 μsec from photographs of the traces. The probe, which was installed on the nozzle centreline, had a cross-sectional area less than 2 % of the nozzle area at any location, and should not have disturbed the flow appreciably.

Also, a flat-plate model with a span and length of 3 in. was used. The angle of the lower surface was 10°, and the leading-edge thickness was approximately 0·001 in. There were two thin-film gauges, mounted on Pyrex disks set into the surface, located 0·9 and 1·9 in. from the leading edge, which supplemented the measurements with the probe. In addition, schlieren photographs revealed the temporal and spatial development of the boundary-layer and shock waves on this model. A conventional off-axis, single-pass schlieren system with 12 in. diameter, 120 in. focal-length mirrors was used for this purpose. The spark light source (commercially built to a design of the National Physical Laboratory) had an arc duration of less than $\frac{1}{2}$ μsec. The light source was triggered after a pre-set delay to investigate various regions of the flow field.

Positive correlation of the timing of events was done in the following manner. The arrival of the incident shock wave at the pressure gauge, $\frac{1}{2}$ in. from the nozzle

entrance, started all the oscilloscope traces, as well as the delay generator that controlled the spark light source. The firing of the spark at a later time created a noticeable disturbance on all traces, and furnished an absolute time reference. The spark time was related to the incident-shock time history by starting a microsec-counter chronometer with the signal from the third shockspeed station (4 in. from the nozzle entrance), and stopping it with an amplified pulse from the spark light source.

Experiments were conducted with incident-shock Mach numbers of 3·0, which produced conditions appropriate to the second case of Smith (1962, 1964), and 5·7, since that is near the value for tailored operation with hydrogen driving nitrogen. The former was done with a driver-gas mixture of 90 % H_2 and 10 % N_2, a driven-gas pressure of 700 mm Hg of nitrogen, and a 0·027 in. aluminium diaphragm. The latter shock speed was produced with a hydrogen driver, 100 mm Hg of nitrogen in the driven tube, and a 0·035 in. aluminium diaphragm. The pressure in the driven section was measured with a Bourdon-type gauge having a range from 0 to 800 mm Hg. The initial pressure in the nozzle and dump tank was set at various values between 36 μ and 50 mm Hg. This chamber was pumped down to a pressure of about 5 μ, then room air was bled in until the desired pressure was obtained. This pressure was measured with both a McLeod gauge and a Pirani gauge.

3.2. *Incident-shock Mach number of* 3·0

The Mach number of the incident shock wave was between 2·90 and 3·10 for all data presented. The theoretical values of pressure and temperature behind the reflected shock wave, as computed from Lewis & Burgess (1964), were 36,000 mm Hg and 1200° K. These values, with a dump-tank pressure of 36 μ Hg, experimentally produced the pressure ratio of $1{\cdot}0 \times 10^6$ and temperature ratio of 4·0 used in the earlier computation (Smith 1962, 1964). A Mach number of 9·96 was computed for the transmitted (primary) shock wave at the nozzle throat from the equations of Alpher & White (1958). Tests were also done with higher dump-tank pressures.

Shock-wave trajectories

Figure 3 contains a comparison of the measured and calculated time histories of the primary and secondary shock waves with an initial pressure of 36 μ Hg. The arrival of the primary shock wave was detected with thin-film heat transfer gauges, as described previously. The secondary shock wave was detected in the nozzle ($x = 4{\cdot}2$ in.) with a Pitot pressure gauge, and downstream of the nozzle exit ($x > 5$ in.) from schlieren photographs. It should be noted that the 'steady-state' model requires the upstream-facing disturbance to be an expansion wave for this pressure ratio, while a shock wave can faintly, but clearly, be seen in the schlieren photographs (see figure 4, plate 1). The effective time at which the measured shock waves left the throat (see figure 3) was about nine microsec. This interval includes the time for the shock wave to travel from the nozzle entrance to the throat, as well as any delay in diaphragm opening.

The measured speed of the primary shock wave seems to be about 10 % higher than the computed speed, which could be caused by imperfect diaphragm breakage, as shown by White (1958). A more probable cause can be found in the work of Bird (1959), where the particular shaping of the converging part of the nozzle was shown to cause large differences in the strength of a transmitted

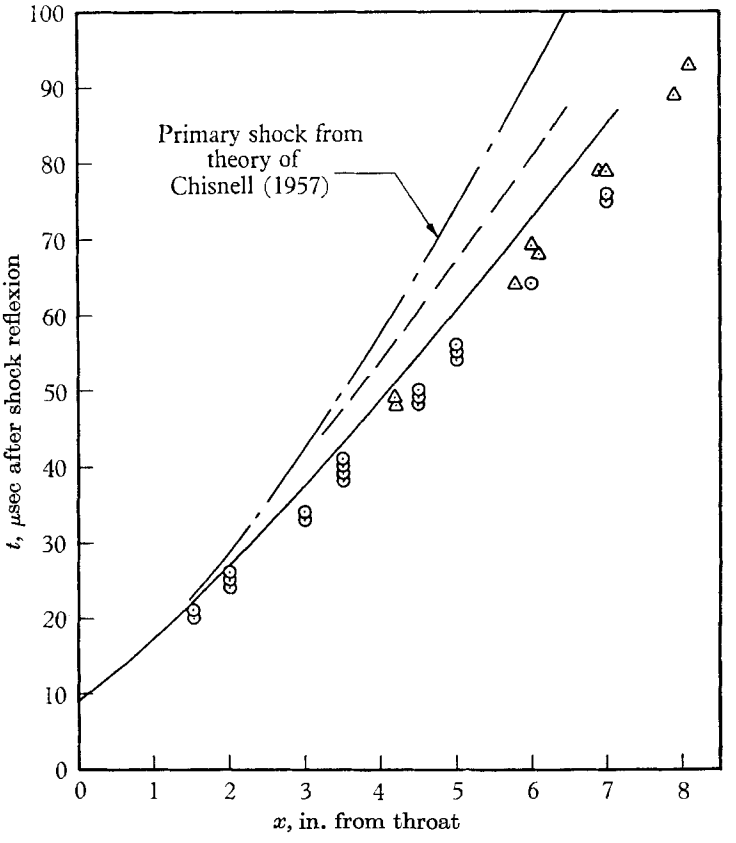

FIGURE 3. Comparison of shock-wave trajectories. Initial pressure = 36 μ Hg, incident-shock Mach number = 3·0. Primary shock wave: ——, numerical calculation; ⊙, experiment. Secondary shock wave: – – –, numerical calculation; △, experiment.

shock wave. His work shows that abrupt changes in channel area cause the strength of a transmitted shock wave to be less than predicted by Alpher & White (1958), while slow, smooth changes can cause transmitted shock waves to be stronger than predicted. The important feature of these measurements is the presence of the secondary shock wave very close behind the primary shock, as predicted by the present flow model. The approximate theory of Chisnell (1957), although not strictly applicable to the present problem, furnishes another prediction of the time history of the primary shock wave. With this theory the speed of the shock wave in the nozzle is even less than the speed from the numerical computations.

Expansion-wave flow

The flow properties in the unsteady expansion-wave region (after the passage of the secondary shock wave) were investigated for dump-tank pressures of 36 μ Hg and 1 mm Hg. The 'steady-state' model requires the upstream-facing disturbance to be an expansion wave for the lower pressure and a shock wave for

Time (μsec)	Mach no.	Reynolds no. per in.	$M^3/R^{\frac{1}{2}}$	$\delta/x^{\frac{1}{2}}$
93	10·5	$1{\cdot}1 \times 10^5$	3·6	0·085
119	8	$1{\cdot}6 \times 10^5$	1·3	0·042
189	6·9	$1{\cdot}8 \times 10^5$	0·8	0·034

TABLE 1

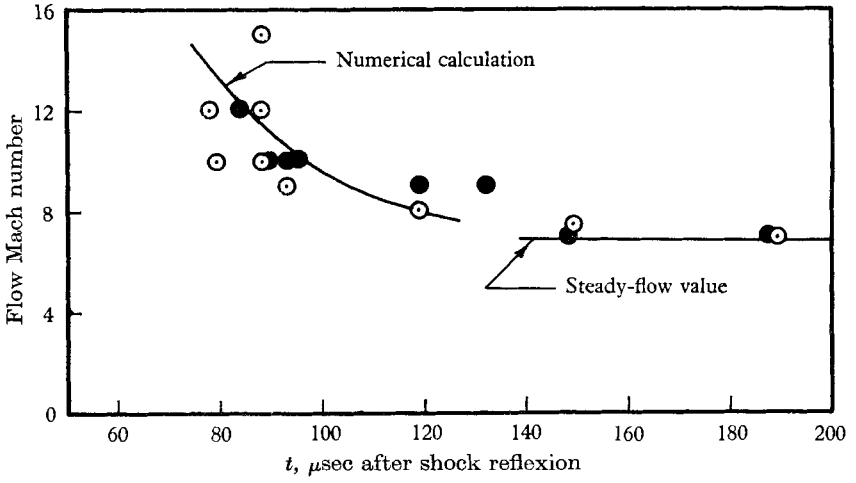

FIGURE 5. Variation of flow Mach number with time at nozzle exit for different initial pressures. Open points signify initial pressure of 36 μ Hg, shaded points, 1 mm Hg.

the higher, which simulates the flow conditions of Holder & Schultz (1962). Although Pitot pressure measurements were made, the results were not conclusive because of the poor signal quality. Consequently, all useful data in this flow region were obtained from the schlieren photographs. Photographs of the unsteady flow over the flat-plate model, taken 93, 119 and 189 μsec after shock reflexion, are shown in figure 4 (plate 1), for the two values of initial pressure. The boundary-layer thickness and the position of the shock wave can be seen to depend more upon the time than the initial pressure. Table 1 contains pertinent flow properties at the nozzle exit from the numerical solutions.

The angle of the shock wave attached to the lower surface of the model was measured in these and other photographs and used to compute the flow Mach number. The effect of the boundary layer on the wedge was estimated, and included in the calculation. The results, compared with the calculated variation of the flow Mach number with time, are shown in figure 5. Agreement is evident, and no influence of initial pressure can be seen.

Further information about the unsteady-flow properties was obtained from measurements of the geometry of flow over the flat plate. These were obtained from the schlieren negatives with a microdensitometer. Traverses were made from the plate surface, through the boundary layer, to the shock wave at eight equally spaced stations. The sample trace shown in figure 6 is a plot of $d\rho/dy$ against y, in which the scale factor for density gradient is not shown, since it

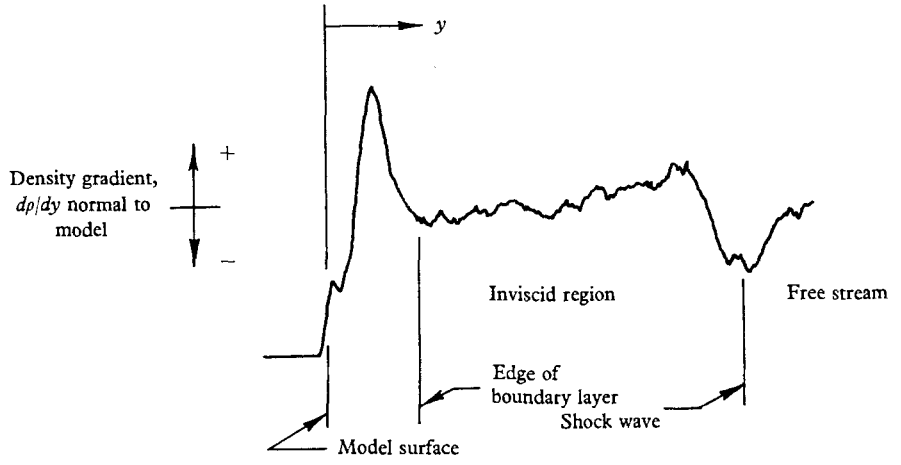

FIGURE 6. Interpretation of densitometer trace of schlieren photographs.

depends on many factors that are imprecisely known. The nearly uniform value inside the shock wave is presumed to be the inviscid region, and the edge of the boundary layer is taken at the point where the uniformity ceases. This point was not easy to choose in all cases, because room air currents disturbed the uniform background in the schlieren photographs, and caused random errors to be present. The distances from the plate surface to the edge of the boundary layer and to the shock wave, as measured from these microdensitometer traces, are shown in figures 7 and 8, respectively. All values of boundary-layer thickness are normalized with $x^{\frac{1}{2}}$. Although there is scatter in the data, the thinning of the boundary layer with time, also observed by Holder & Schultz (1962), can be seen.

The theoretical thickness of the boundary layer during the transient flow was computed utilizing the values of Mach number and Reynolds number at the nozzle exit in table 1. Conical-flow effects were neglected, a linear viscosity-temperature relation was used, and the Prandtl number was assumed to be unity. The methods outlined by Stewartson (1964) were followed, and the thickness of a compressible laminar boundary layer on a cold flat plate was found to be

$$\delta/x = (1/R_x^{\frac{1}{2}})[\eta^* + 0{\cdot}332(\gamma-1)M_e^2 + 1{\cdot}730\{(T_w/T_e)-1\}]. \tag{8}$$

The value of η^* which comes from the incompressible boundary-layer solution was taken as 5·0, corresponding to the location where the velocity is 0·99 of the external value. Table 1 and figure 7 contain values of $\delta/x^{\frac{1}{2}}$ computed with this equation.

Although the boundary-layer thickness changed by more than a factor of two during the transient flow, there seems to be little, if any, dependence on the initial pressure in the nozzle. The growth of the boundary layer with distance was

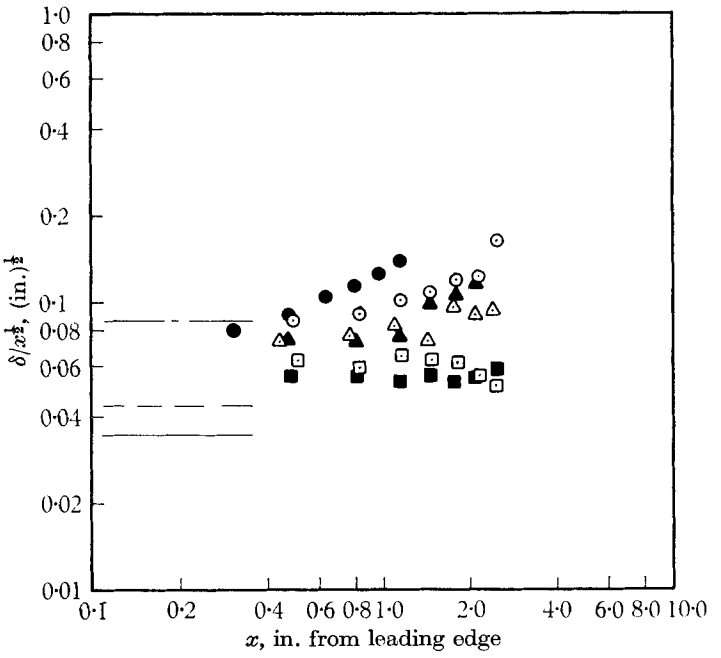

FIGURE 7. Variation of flat-plate boundary-layer thickness with time for different initial pressures. Open points signify initial pressure of 36 μ Hg, shaded points, 1 mm Hg.

Quasi-steady theory	Experiment	Time (μsec)
— — —	⊙	93
- - - - -	△	119
———	⊡	189

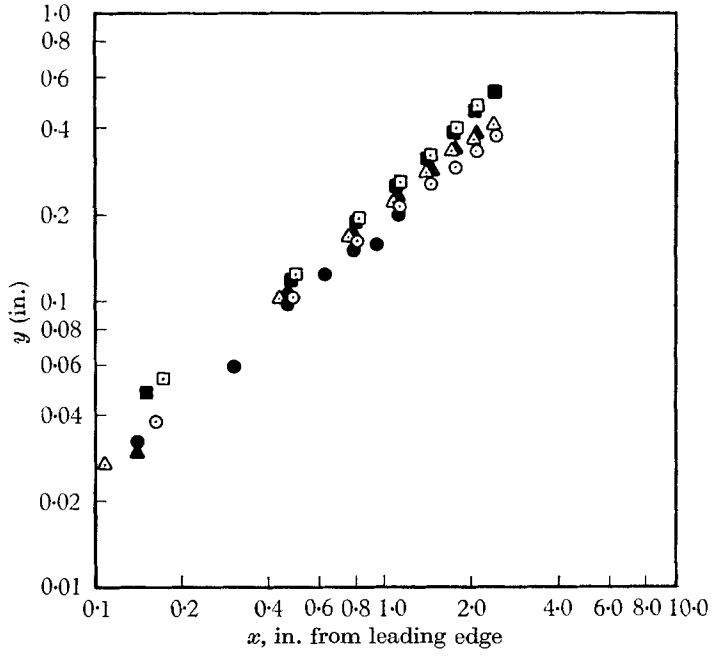

FIGURE 8. Variation of flat-plate shock-wave shape with time for different initial pressures. Open points signify initial pressure of 36 μ Hg, shaded points, 1 mm Hg. Time: ⊙, 93 μsec; ⊡, 119 μsec; △, 189 μsec.

greater than predicted from a uniform-flow theory, and can be ascribed to the conical-flow effects. At early times, this seems to be augmented by the presence of the secondary shock wave and the accompanying adverse pressure gradient.

The possible effects of flow unsteadiness, as well as flow separation and subsequent reattachment, were assessed for the test conditions. Moore (1951) showed that an unsteady laminar boundary layer can be considered as quasi-steady, providing the parameter $x(du/dt)/u^2$ is small. In the present case the value of this parameter, as evaluated from the numerical solutions, was less than 0·2 for all times greater than 60 μsec. Consequently, the boundary layer on the flat plate may be considered as quasi-steady, with its thickness determined by the instantaneous values of flow Mach number and Reynolds number. Since the leading edge of the flat plate was sharp, the shape of the shock wave was dominated by the thickness of the boundary layer rather than model bluntness. The data in figure 8 show that flow separation did not occur, because the shock wave moved *away* from the plate as the boundary layer thinned with increasing time. The behaviour of the boundary layer and shock wave are consistent with a transient flow having a Mach number that is higher, and a Reynolds number lower, than the respective steady-flow values.

Effects of initial pressure

The effect of still higher initial pressures on the trajectory of the secondary shock wave, and ultimate failure of the nozzle to start was investigated. For the present conditions the steady-flow static pressure at the nozzle exit ($x = 5{\cdot}0$ in.) was about 10 mm Hg. Consequently, additional tests were done with initial pressures of 5 and 50 mm Hg. Figure 9 is an x–t diagram of the results with initial pressure ranging from 36 μ to 50 mm Hg. Also shown is the path of the $(u–a)$ characteristic for steady flow, computed from equation 7. It can be seen that the secondary shock wave passed by the nozzle exit before the $(u–a)$ characteristic for all initial pressures except the highest. Even then, there was a loss of only 10 μsec of useful testing time. From these results it can be seen that the growth of the secondary shock wave will cause a loss of testing time only if the initial pressure is significantly higher than the steady-flow static pressure.

Schlieren photographs at 5 and 50 mm Hg are shown in figure 10 (plate 2). At 5 mm Hg the nozzle started satisfactorily, and was not adversely affected by the initial pressure. However, at 50 mm Hg the high initial pressure caused the nozzle boundary layer to separate, and produced strong oblique shock waves. If the initial pressure was increased still more, the failure of the nozzle to start would be caused by boundary-layer separation and the related two-dimensional flow, rather than by any tendency of the secondary shock wave to slow down and stop in the nozzle. It seems that the assumption of one-dimensional inviscid flow is violated soon after the initial pressure exceeds the steady-flow static pressure.

3.3. *Incident-shock Mach number of* 5·7

The Mach number of the incident-shock wave was between 5·6 and 5·8 for all data presented. The theoretical values of pressure and temperature behind the reflected shock wave, as computed from Lewis & Burgess (1964), are

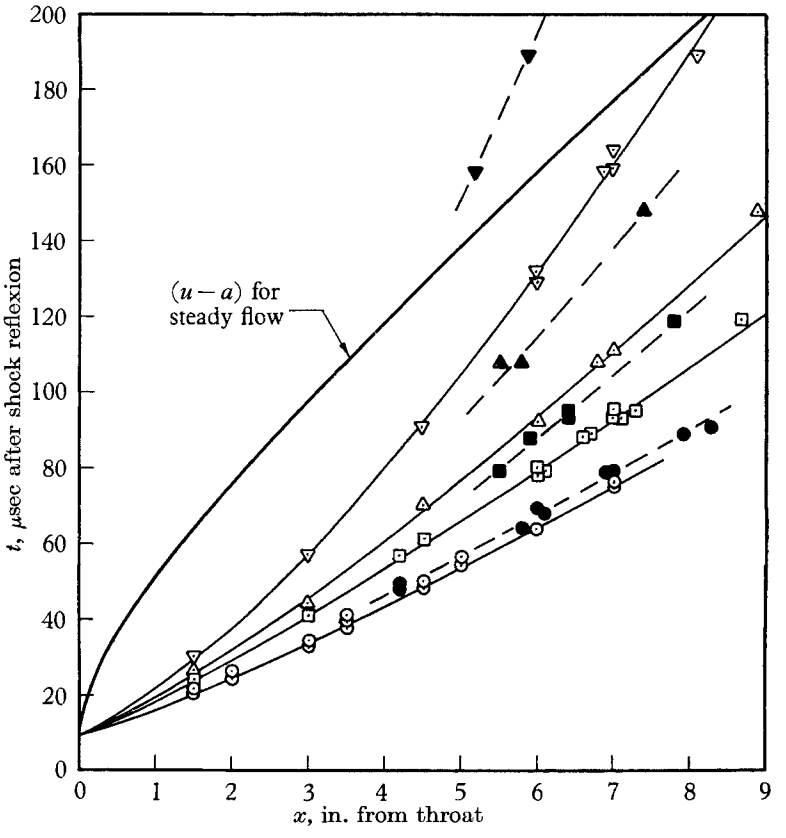

FIGURE 9. Shock-wave trajectories for various initial pressures. Incident-shock Mach number = 3·0. Open points signify primary shock wave, shaded points, secondary shock wave. Initial pressures: ⊙, 36 μ Hg; ⊡, 1 mm Hg; △, 5 mm Hg; ▽, 50 mm Hg.

29,000 mm Hg and 3700° K. The corresponding steady-flow static pressure at the nozzle exit is about 8 mm Hg.

Effects of initial pressure

Figure 11 contains the measured trajectories of the primary and secondary shock waves for initial pressures of 1, 5 and 30 mm Hg, as well as the steady-flow characteristic from equation (7). The effective time at which the shock waves left the throat was about four microsec for this case. The overall appearance of these data is similar to the data in figure 9, except that the time axis is compressed because of the higher stagnation temperature. At the nozzle exit, the secondary shock wave caused a loss of testing time only for the 30 mm Hg case, and this loss was about 40 μsec. Schlieren photographs revealed oblique shock waves caused by separation of the nozzle boundary layer at this high initial pressure, as were observed in the tests with a lower incident-shock Mach number. For these conditions, initial nozzle pressures up to the steady-flow static pressure do not cause a loss of testing time, despite the presence of a strong secondary shock wave.

Although tests were not done with higher incident-shock Mach numbers, the effects are predictable. The higher temperatures in the reflected-shock region will

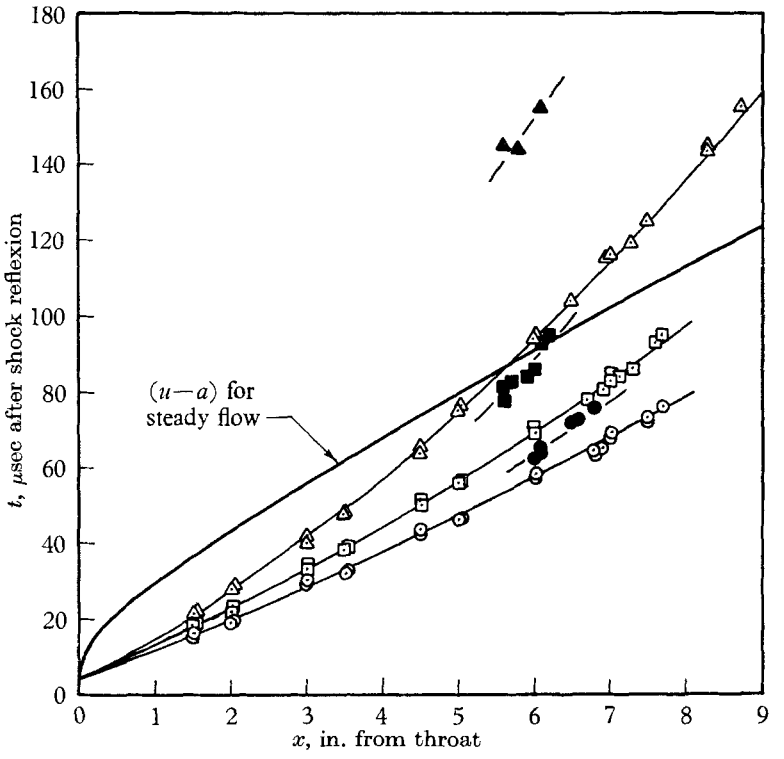

FIGURE 11. Shock-wave trajectories for various initial pressures. Incident-shock Mach number = 5·7. Open points signify primary shock wave, shaded points, secondary shock wave. Initial pressure: ⊙, 1 mm Hg; ⊡, 5 mm Hg; △, 30 mm Hg.

cause the $(u-a)$ characteristic to arrive even sooner, as a result of the inverse dependence on a_5 in equation (7). Since the speed of the primary (transmitted) shock wave does not increase proportionately, a loss of testing time will possibly occur. Initial pressures lower than the steady-flow static pressure are necessary to prevent loss of testing time under conditions of high stagnation temperatures.

4. Conclusions

An experimental study has revealed the flow properties during the starting process in a shock-tunnel nozzle. The measurements corroborate earlier calculations of the flow field (Smith 1962, 1964), and verify the conclusions that an unsteady expansion wave dominates the transient flow, and the shock-wave system plays a minor role. It is demonstrated that the thinning of the boundary layer on a flat plate during the transient flow, reported by Holder & Schultz (1962) was caused by flow in this expansion region. A comparison with the more detailed calculations and the experimental data reveals the shortcomings of the 'steady-state' model of the nozzle starting process. It is pessimistic, especially regarding the initial pressure that can be tolerated in the nozzle without a loss of testing time. The secondary shock wave is in the wrong location in the 'steady-state' model, and the structure of the flow field during the transient flow is incorrectly predicted. The present study indicates that initial pressures up to the

steady-flow static pressure do not cause any loss of testing time if the stagnation temperature is less than about 3500° K. For higher temperatures it is necessary to use lower initial pressures to assure minimum starting times.

This experimental work was supported in part by a NATO Postdoctoral Fellowship in Science, and some of the capital equipment was provided by a grant from the Science Research Council. The author wishes to express his appreciation and gratitude to all those individuals in the Department of Engineering Science who contributed to this study: to Professor D. W. Holder for providing space and equipment for the experimental study; to Prof. Holder and Drs C. L. Brundin, D. W. Schultz and D. A. Spence for helpful discussions and criticism; and to Mr A. J. Woolgar for the design of electronic circuits.

REFERENCES

ACKROYD, J. A. D. 1964 Studies on the running time in a shock tube and shock tunnel. Ph.D. Thesis, University of London.

ALPHER, R. A. & WHITE, D. R. 1958 Flow in shock tubes with area change at the diaphragm section. *J. Fluid Mech.* **3**, 457.

BIRD, G. A. 1959 The effect of wall shape on the degree of reinforcement of a shock wave moving into a converging channel. *J. Fluid Mech.* **5**, 60.

CHESTER, W. 1960 The propagation of shock waves along ducts of varying cross-section. *Advances in Applied Mechanics, VI*, p. 119. New York: Academic Press.

CHISNELL, R. F. 1957 The motion of a shock wave in a channel, with applications to cylindrical and spherical shock waves. *J. Fluid Mech.* **2**, 286.

GLASS, I. I. & HALL, J. G. 1959 *Handbook of Supersonic Aerodynamics*, §18: Shock tubes. *NAVORD Rep.* no. 1488 (vol. 6).

GLICK, H. S., HERTZBERG, A. & SMITH, W. E. 1955 Flow phenomena in starting a hypersonic shock tunnel. *Cornell Aero Lab. Rep.* no. AD-789-A-3.

HENSHALL, B. D. 1960 Experimental results from the NPL hypersonic shock tunnel *Hypersonic Flow, Colston Papers.* London: Butterworths.

HENSHALL, B. D. & GADD, G. E. 1956 Factors affecting the performance of the nozzle of a hypersonic shock tube. *ARC CP* 293.

HERTZBERG, A. 1956 The application of the shock tube to the study of the problems of hypersonic flight. *Jet Propulsion*, **26**, 549.

HOLDER, D. W. & SCHULTZ, D. L. 1962 The duration and properties of the flow in a hypersonic shock tunnel. *Hypersonic Flow Research, Prog. in Astronautics and Rocketry* (vol. 7). New York: Academic Press.

LEWIS, C. H. & BURGESS, E. G. 1964 Charts of normal shock wave properties in imperfect nitrogen. Arnold Engineering Development Center, *Rep.* no. AEDC-TDR-64-104.

MOORE, F. K. 1951 Unsteady laminar boundary-layer flow. *NACA TN* 2471.

PARKS, E. K. 1952 Supersonic flow in a shock tube of divergent cross-section. Univ. of Toronto, *UTIA Rep.* no. 18.

SMITH, C. E. 1962 An analytic study of the starting process in a hypersonic nozzle. Ph.D. Thesis, Stanford Univ.

SMITH, C. E. 1964 An analytic study of the starting process in a hypersonic nozzle. *Proc. of Heat Transfer and Fluid Mech. Institute*, p. 198. Stanford Univ. Press.

STEWARTSON, K. 1964 *The Theory of Laminar Boundary Layers in Compressible Fluids.* Oxford: Clarendon Press.

WHITE, D. R. 1958 Influence of diaphragm opening time on shock-tube flows. *J. Fluid Mech.* **4**, 585.

WITTLIFF, C. E., WILSON, M. R. & HERTZBERG, A. 1959 The tailored-interface hypersonic shock tunnel. *J. Aero. Sci.* **26**, 219.

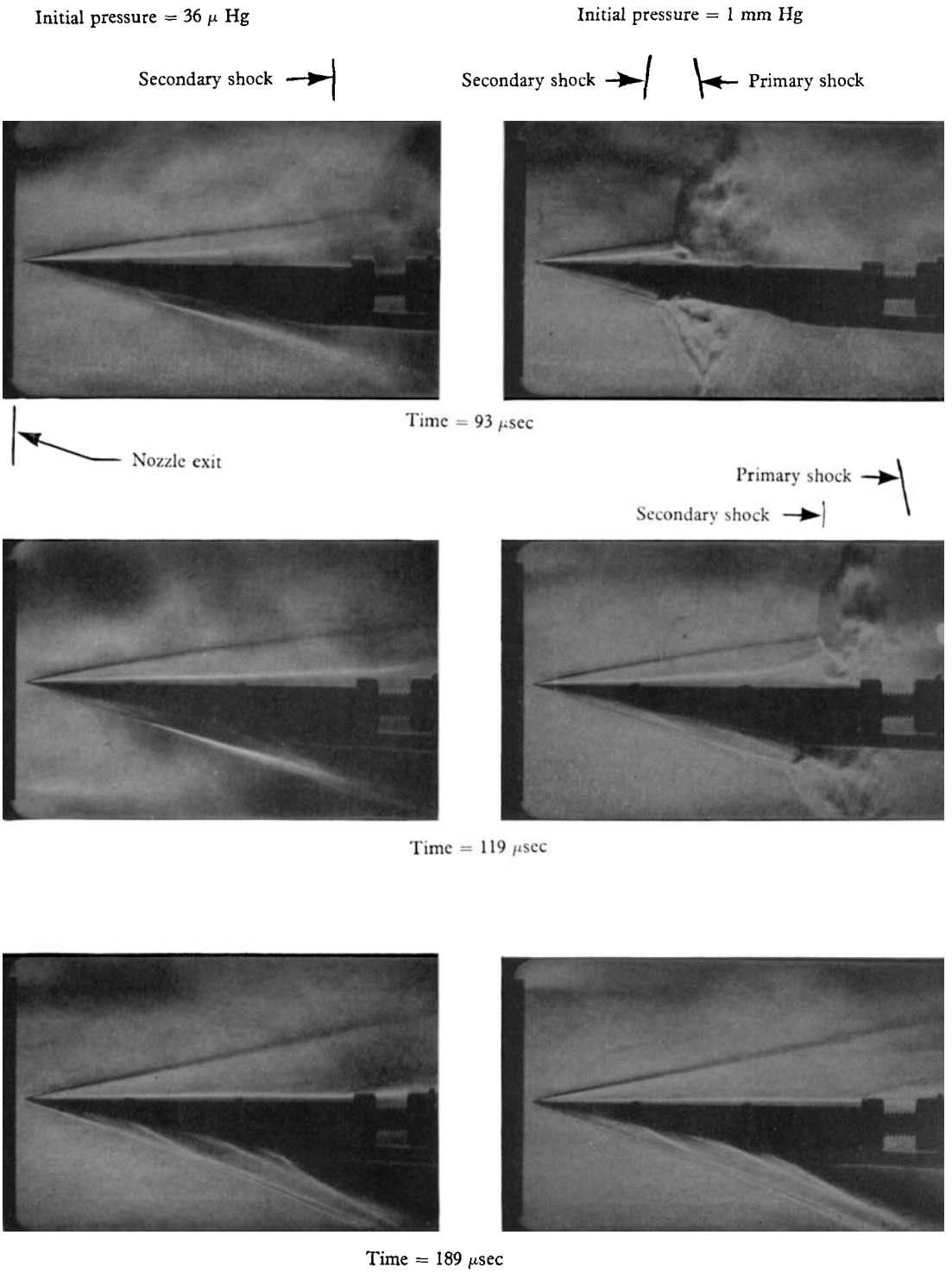

FIGURE 4. Schlieren photographs of model at various times during the nozzle starting process.

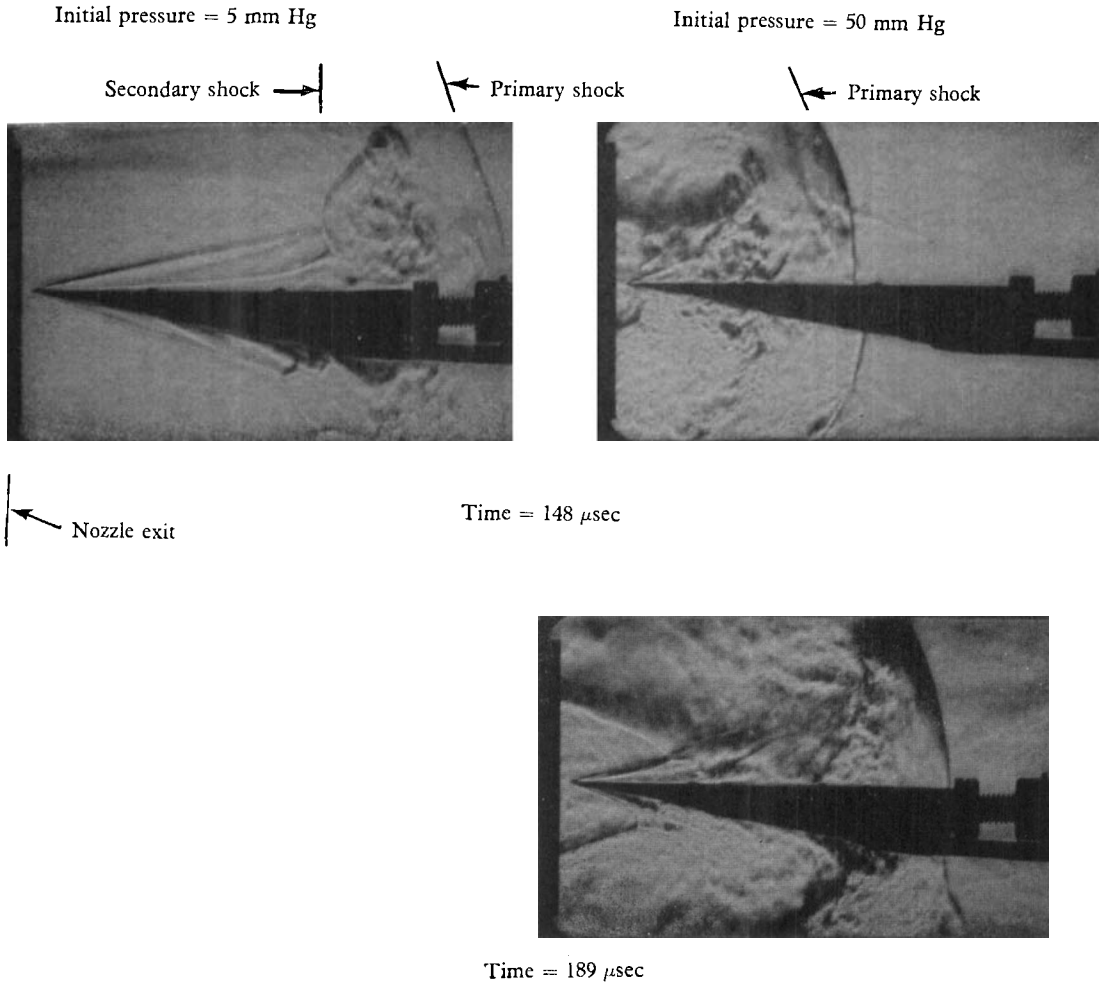

FIGURE 10. Schlieren photographs of starting process with high initial pressures.